Ocean Dynamics (2021) 71:981–992
https://doi.org/10.1007/s10236-021-01478-5

Effect of the wind acceleration magnitude during the first stages of the wind-wave generation process

Lucia Robles-Diaz[1] · Francisco J. Ocampo-Torres[1] · Hubert Branger[2] · Hector Garcia-Nava[3] · Pedro Osuna[1] · Nicolas Rascle[1]

Received: 10 September 2020 / Accepted: 27 July 2021 / Published online: 17 August 2021

Abstract

A comprehensive analysis of the wavefield evolution under accelerated wind conditions provides an essential contribution to understanding the wind-wave generation process. A set of experiments was carried out in a large wind-wave facility where it is possible to reproduce high wind speed conditions to study the wind acceleration effect in the wind-wave development. The facility was equipped with high-frequency sampling devices that provide accurate air turbulence and water surface displacement measurements. From this deployment, it was possible to describe the evolution of the wave characteristics under different magnitudes of constant wind acceleration in detail. This study analyzes the wind acceleration effect in the early stages of wind-wave generation and evolution. The increase of spectrum energy saturation level and the downshift of the peak frequency are processes associated with the spectral shape evolution under low acceleration wind conditions. Under high wind acceleration conditions, the spectral shape did not vary with wind speed and fetch. Despite under low acceleration wind conditions, the wavefield is more developed than under high acceleration wind conditions; there was no direct relation between wind acceleration and the wavefield efficiency to grow. Besides, during these early instants, it was observed that a more developed wave field, associated with low acceleration wind conditions, could slow down the increase of drag coefficient with wind speed.

Keywords Incipient wave generation · Accelerated wind · Spectral shape evolution · Wave age

This article is part of the Topical Collection on the *International Conference of Marine Science ICMS2018, the 3rd Latin American Symposium on Water Waves (LatWaves 2018), Medellin, Colombia, 19–23 November 2018 and the XVIII National Seminar on Marine Sciences and Technologies (SENALMAR), Barranquilla, Colombia 22–25 October 2019*

Responsible Editor: Nelson Violante-Carvalho

✉ Lucia Robles-Diaz
lrobles@cicese.edu.mx

[1] Departamento de Oceanografía Física, Centro de Investigación Científica y de Educación Superior de Ensenada, Ensenada, Mexico

[2] Aix-Marseille Univ, CNRS, Centrale Marseille, IRPHE, Marseille, France

[3] Instituto de Investigaciones Oceanológicas, Universidad Autónoma de Baja California, Ensenada, Mexico

1 Introduction

The mechanics controlling wind-wave generation has been widely studied in the last decades (Jeffreys 1925; Phillips 1957; Miles 1957). Also, a quasi-linear theory of the interaction of wind and waves was elaborated (Fabrikant 1976; Janssen 1982). However, in those early works, constant wind speed conditions were typically assumed during the wind-wave field generation process. Later on, the wind-wave generation process as the result of a quickly and abruptly starting wind field before reaching constant wind conditions was described. From one of these studies, an exponential behavior of the wave field growth rate, as resulted from a wind that suddenly started to blow, was suggested (Mitsuyasu and Rikiishi 1978). The wavefield evolution generated after a suddenly starting wind, from an experimental and theoretical study, was reported (Kawai

1979). The exponential wave field growth was discussed upon the dependence on the friction velocity.

Besides, the behavior of the wave spectrum under accelerated wind speed conditions was investigated by Toba et al. (1988). It was shown that the spectral tail energy level decreases under accelerated wind conditions compared to decelerating wind conditions. It was also stated that the peak of the spectrum gets broader under the accelerated wind. Furthermore, under slightly fluctuating wind conditions, it was found that modifications on the roughness length induce changes in the energy saturation level of the wind-wave spectrum and that the relation between the dimensionless roughness length parameter and the wave age is modified (Toba and Ebuchi 1991). The wave spectrum evolution resulting after an abrupt onset of the wind was also characterized by Waseda et al. (2001). In that study, it was reported that the response of the wavefield occurs in two different time scales, one determined by the local equilibrium and the other one by the fetch. Recently, a set of controlled experiments were carried out in a wind-wave flume to study the evolution of the wavefield generated under a quick and abrupt onset of wind, followed by constant wind conditions (Zavadsky and Shemer 2017). From that study, four stages during the wavefield evolution were distinguished after that impulsive wind forcing. At first, the initial short waves grow fast, followed by a remarkable decrease in the growth rate. Then, the growth rate was shown to be relatively constant, and it increased some seconds again before the quasi-steady state was reached.

A detailed description of how, during the early stages of wind-wave generation, the wind acceleration magnitude affects the air turbulent boundary layer evolution, the momentum availability, and the wind-wave growth was given in Robles-Diaz et al. (2019). The present analysis aims to provide a detailed description of the effect of wind acceleration in the momentum transfer through the air-sea interface by analyzing the wind-wave spectral shape. It is also possible to link the evolution of the drag coefficient with the wavefield characteristics when considering that the wind increases under various acceleration conditions. The rest of the paper is organized as follows: the characteristics of the experimental facility and the measurement devices, and the experimental runs, are described in Section 2. A detailed spectral analysis of the water surface elevation is presented in Section 3. The time series analysis of the wave field parameters, as well as the behavior of the wave growth rate is given in Section 4. The relation between the drag coefficient with both wave age and wind speed is analyzed in Section 5, and finally, a summary of the main findings is given in Section 6.

2 Experimental design and procedures

2.1 Facility and measuring devices

Laboratory experiments were carried out in the *IRPHE/Institut Pythéas* large wind-wave facility in Marseille, France. The facility consists of a water tank of 40 m long, 2.6 m wide, and 1 m deep, and an air section of 50 m long, 3 m wide, and 1.6 m high (Fig. 1). A description of the facility can be found in Coantic et al. (1981), and at the address http://www.pytheas.univ-amu.fr/?-LASIF-Grande-Soufflerie-air-eau-de-Luminy-. Further details and full description are included in Robles-Diaz et al. (2019)

This facility is a closed-loop flume that minimizes the spatial variations of wind speed along the flume compared to an open-loop facility. These characteristics make it more suitable to carry out wave generation experiments under stable and accelerated wind conditions. The desired variations of wind speed as a function of time were controlled with a computer under a coupled Matlab/Labview real-time control software that allows reproducing the same wind conditions several times. This computer system is a handy tool for repeating the experiments and increasing the results statistical significance. Each experiment was repeated three times.

During the laboratory experiments, the wind-wave flume was instrumented with several devices along 11 measuring stations. In the water part, resistance wires were installed at each station. At stations 1, 2, and 7, capacitance wires were also installed. Both types of devices provide measurements

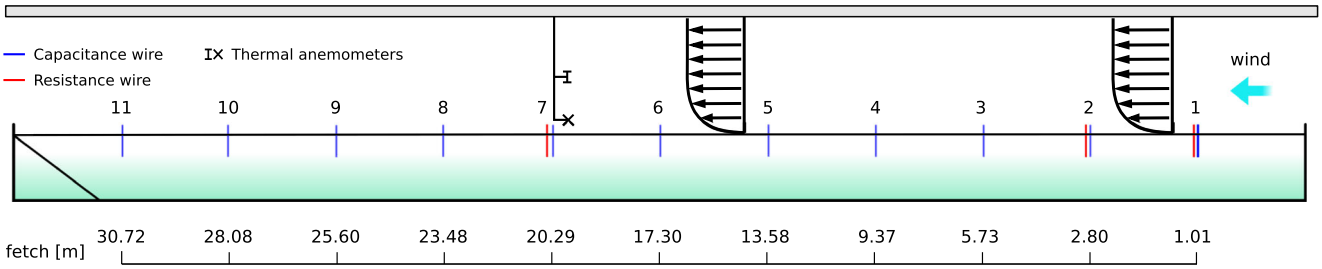

Fig. 1 Layout of the Institut Pythéas wind-wave facility (not to scale), where the measuring station locations are depicted

of the free surface displacement with a high sampling frequency of 256 Hz. A hot wire probe and an X wire probe were installed at station 7 to measure the mean and turbulent wind flow. The hot wire probe and the X wire probe were located at 0.720 m and 0.145 m height from the mean free surface.

2.2 Experimental runs

A series of experiments were designed to characterize the initial stages of wind-wave generation under constant acceleration wind conditions. For each experimental run, a specific wind acceleration was imposed. Each experiment started with a constant low wind speed period, followed by a constant wind acceleration period. Each experiment has its specific acceleration value that defines the period of measurements, mainly dealing with this work. For instance, experiment 1 presents low acceleration, experiments 2, 3, and 4 present moderate-low, moderate and moderate-high acceleration, and the high acceleration belongs to experiment 5. At the end of the acceleration period, all the experiments reached a maximum and stable wind speed of 13 m s^{-1}. The acceleration period duration differed depending upon the wind acceleration value to reach this wind speed of 13 m s^{-1}. The history of wind speed in the five experiments, measured at station 7, and used for the present work analysis, is shown in Fig. 2.

The mean wind speed is extrapolated to 10 m wind speed, U_{10}, to compare some results with another previous analysis. U_{10} was estimated assuming neutral conditions and a logarithmic wind profile, from $U_{10} = U_{ref} + (u_*/\kappa)\ln(10/z_{ref})$; where z_{ref} is the height where the single wire anemometer was located, U_{ref} is the mean wind speed, u_* is the friction velocity estimated from eddy covariance method, and κ is the Von Kármán constant.

3 Spectral analysis

To characterized the wave development under different acceleration regimes, a series of frequency power spectra

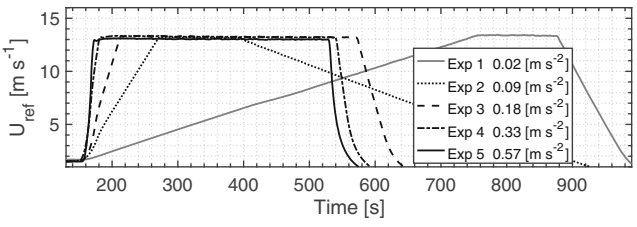

Fig. 2 Mean wind speed at z = 0.72 m, U_{ref}, as a function of time during the 5 selected experiments, measured at station 7. Each line corresponds to a particular experiment with a characteristic acceleration value as indicated in the inset box

of the water surface elevation was estimated from the measurements obtained under accelerated wind conditions in each experimental run. In this analysis, a sliding window of 8 s (2048 data points) was used to estimate each spectrum, assuming that during this 8 s period, the surface elevation fluctuations were somehow relatively well represented under quasi-steady conditions. Wave spectra were computed after applying a Blackman-Harris window in each 8 s data series. The resulting frequency resolution of the spectrum is $\Delta f = 0.125$ Hz. The spectra were computed with 10 degrees of freedom. The confidence interval was estimated by inverse chi-square distribution. Since the data acquisition rate is 256 Hz, in each calculated power spectrum the nominal Nyquist frequency is 128 Hz.

The evolution of the surface wave power spectrum as a function of wind speed, U, is shown in Fig. 3. These results correspond to station 7, located in the middle of the water tank with a fetch of 20.29 m. This station is the only one where the two thermal anemometers measured the wind speed. In each row, the spectra evolution for each experiment is shown. From the upper to the lower row, the acceleration associated with each experiment increases. The upper row belongs to the experiment with the lowest acceleration. The lower row belongs to the experiment with the highest acceleration. The spectrum evolution with increasing wind speed can be followed in each row under the different panel columns (increasing wind speed from left to right). The constant wind condition spectra associated with 6, 9.5, and 13 m s^{-1} are also shown as a reference. The $1.5 f_p$ limit and the confidence interval are included. The spectral saturation level proposed by Phillips (1958) and Toba (1973) is included. Phillips formulation is always plotted at the same energy level, as it only depends on gravitational acceleration. It can be used as a reference to compare high frequencies spectral energy levels between experiments and different wind speed conditions.

The spectra associated with accelerated wind conditions reach the spectral shape observed under constant wind conditions, under low acceleration wind conditions (experiment 1). As wind acceleration increases for the other experiments, the expected spectral shape for a given constant wind speed is not reached under accelerated wind conditions. This fact indicates that time is a limiting factor that should be considered when a wave field is evolving under accelerated wind conditions. However, the acceleration is also determining the spectral shape evolution. As wind speed increases, an increase of the energy saturation level in the high-frequency spectral tail, jointly with a characteristic downshifting of the peak frequency, is noticed under the low and moderate-low acceleration wind conditions, experiments 1 and 2. An increase of the energy saturation level in the high-frequency spectral tail with wind speed is observed under moderate-high and high acceleration wind conditions, experiments

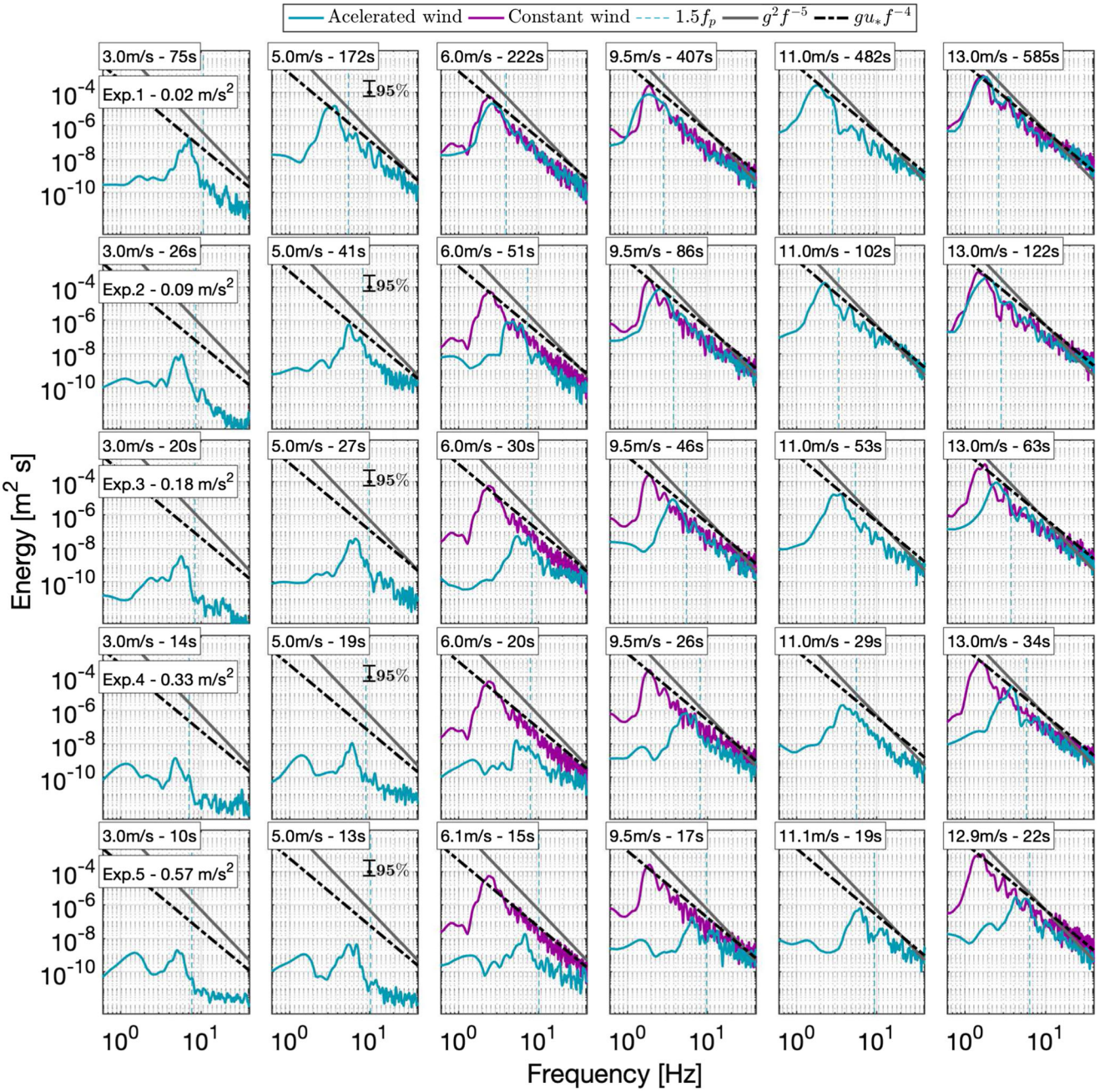

Fig. 3 Wave energy spectrum evolution with wind speed for each experiment at station 7. The spectra associated with 6, 9.5, and 13 m s^{-1} constant wind speed conditions are included in purple. The solid gray line corresponds to Phillips (1958) formulation, $g^2 f^{-5}$. The dotted black line corresponds to Toba (1973) formulation, $gu_* f^{-4}$. The dotted blue line indicates the $1.5 f_p$ limit. The acceleration associated with each experiment is shown. The mean wind speed and time-lapse from the beginning of the acceleration period associated with each panel are included

4 and 5. Still, it is not as remarkable as the one seen under low and moderate-low acceleration wind conditions, for low wind speeds. Nevertheless, no spectral peak frequency downshifting is observed under high acceleration wind conditions (experiment 5), together with the increase of high-frequency energy saturation level (Fig. 3).

The analysis of the spectra evolution is quantitatively supported with data presented in Tables 1 and 2. The peak frequency and its associated energy of the spectra corresponding to the maximum wind speed are shown in Table 1, as obtained in each experiment (columns), at six stations along the flume (rows). Then, it can be observed that under maximum wind speed, the lowest peak frequencies are associated with low and moderate-low acceleration wind conditions (experiments 1 and 2). The spectral energy density, E, of the 15 Hz frequency

Table 1 Spectral peak frequency, f_p, and its associated spectral energy density, E_p, under maximum wind speed of 13 m s^{-1}, estimated from measurements at stations 1, 3, 5, 7, 9, and 11, of experiments 1 to 5

Station	f_p [Hz] / E [m^2 s]	Exp. 1	Exp. 2	Exp. 3	Exp. 4	Exp. 5
St. 1	f_p	4.25	4.38	5.01	4.38	3.88
	E	8.36e-06	1.27e-05	8.59e-06	6.97e-06	4.34e-06
St. 3	f_p	2.38	3.00	2.88	3.63	5.13
	E	4.04e-05	8.79e-05	1.23e-05	1.47e-05	1.66e-06
St. 5	f_p	2.00	2.25	2.25	3.88	5.51
	E	4.88e-04	9.71e-05	2.75e-04	1.10e-05	1.60e-06
St. 7	f_p	1.75	1.88	2.50	3.88	4.25
	E	8.46e-04	3.55e-04	8.75e-05	2.67e-05	2.94e-06
St. 9	f_p	1.50	1.63	2.50	3.13	4.38
	E	8.09e-04	1.39e-04	1.70e-04	2.62e-05	1.02e-05
St. 11	f_p	1.50	1.75	2.38	3.13	4.63
	E	9.22e-04	6.03e-04	1.55e-04	3.10e-05	6.37e-06

is shown in Table 2, as estimated in each experiment (columns), and the six stations along the tank (rows). 15 Hz frequency energy was used to reference the energy level of the spectral tail and compare this energy level between experiments. At Table 2, the E_6, $E_{9.5}$, and E_{13} values correspond to the energy level associated with the 15 Hz frequency of the spectra under 6 m s^{-1}, 9.5 m s^{-1}, and 13 m s^{-1} wind speeds, respectively. Thus, it is also possible to observe the change of the 15 Hz energy levels with wind speed. The saturation range of the spectral energy density is lower under high acceleration wind conditions compared to those low acceleration cases, under low wind speed

Table 2 Spectral energy density associated to the 15 Hz frequency under wind speeds of 6, 9.5, and 13 m s^{-1} (indicated as E_6, $E_{9.5}$, and E_{13}), estimated from measurements at stations 1, 3, 5, 7, 9, and 11, of experiments 1 to 5

Station	E [m^2 s]	Exp. 1	Exp. 2	Exp. 3	Exp. 4	Exp. 5
1	E_6	1.58e-08	1.62e-08	8.93e-09	1.47e-09	8.13e-09
	$E_{9.5}$	5.67e-09	9.07e-10	5.49e-09	2.44e-08	2.52e-08
	E_{13}	2.23e-08	1.26e-07	3.47e-08	1.33e-08	9.57e-09
3	E_6	1.21e-09	1.20e-09	6.75e-10	4.76e-10	4.56e-10
	$E_{9.5}$	2.75e-09	2.02e-09	3.17e-09	1.92e-09	1.90e-09
	E_{13}	1.73e-08	4.05e-08	1.21e-08	1.23e-08	1.06e-08
5	E_6	7.12e-10	7.01e-10	1.36e-09	1.33e-10	1.45e-10
	$E_{9.5}$	1.76e-09	2.32e-09	1.81e-09	1.26e-09	1.87e-09
	E_{13}	2.16e-08	1.13e-08	2.51e-08	7.50e-09	5.99e-09
7	E_6	7.87e-09	6.78e-10	4.64e-10	3.01e-10	1.03e-10
	$E_{9.5}$	2.96e-09	1.07e-08	8.58e-10	4.16e-09	1.32e-09
	E_{13}	4.56e-08	5.13e-08	1.91e-08	5.96e-09	1.37e-08
9	E_6	8.18e-10	3.54e-10	4.48e-10	1.25e-10	5.08e-10
	$E_{9.5}$	3.05e-09	9.24e-10	2.81e-09	1.43e-09	1.24e-09
	E_{13}	4.59e-08	2.04e-08	2.15e-08	3.41e-08	1.02e-08
11	E_6	4.38e-10	2.57e-10	1.69e-10	4.80e-10	2.03e-10
	$E_{9.5}$	4.77e-10	6.07e-10	2.04e-09	1.77e-09	1.54e-09
	E_{13}	9.78e-09	1.07e-08	7.23e-09	1.18e-08	2.56e-09

conditions. These findings imply that waves associated with those frequencies are steeper under low acceleration wind conditions than high acceleration wind conditions under similar wind speed conditions. From the data of Tables 1 and 2 it is possible to confirm the observations made from Fig. 3. Despite the energy level of the saturation rage is increasing with wind speed, the downshift of peak frequency is not remarkable under high acceleration wind conditions. These results show that the time and the wind acceleration affect the spectral shape evolution with wind speed.

In several studies, the shape of the high-frequency tail of the spectrum has been described. The hypothesis that wave breaking limits the spectral energy level associated with high frequencies was posed by Phillips (1958). The gravitational acceleration is the parameter dominating wave breaking, and the spectral energy density for deepwater conditions results in $E(f) \sim g^2 f^{-5}$. The effect of the wind controlling the tail shape was included by Toba (1973), introducing wind stress in the formulation, hence $E(f) \sim g u_* f^{-4}$. In Fig. 3, it is possible to distinguish a particular slope in the tail of the spectrum for frequencies higher than $1.5 f_p$ ($f \geq 1.5 f_p$ is indicated as dashed blue line). The spectral tail shape is better described with a lower power-law than f^{-5}, relatively closer to Toba's decay law, in the majority of the spectra observed in Fig. 3. As wind speed increases, the energy density decay rate of high frequencies becomes higher, and these changes are described adequately with the inclusion of u_* in the formulation of the spectral energy density.

The evolution of the spectral energy density as a function of fetch is shown in Fig. 4, where the spectra associated with the 13 m s^{-1} maximum wind speed are shown as the result of the measurements at five stations along the water tank (stations 1, 3, 5, 7, and 11). The spectra evolution with fetch under constant wind conditions of 13 m s^{-1} was also computed (not shown). The spectral shape evolution with fetch under low acceleration wind conditions (experiment 1) is similar to the spectral shape evolution under constant wind conditions of 13 m s^{-1} wind speed. Similar results were observed in Fig. 3, for the spectral shape evolution with wind speed. Then, under low acceleration wind conditions, the spectral shape evolution with wind speed and fetch is not influenced by the wind acceleration. The acceleration magnitude affects the wave development with fetch under the rest of the acceleration wind conditions, compared to constant wind conditions. A readily apparent peak frequency downshift enhanced process with fetch is noticeable under low, moderate-low, and moderate acceleration wind conditions. These characteristics of surface elevation spectra, as obtained from measurements at the various stations along the flume, can also be observed from the data given in Table 1. There is no remarkable difference in the spectral energy level of saturation range frequencies with fetch. These observations are supported from data presented in Table 2. However, the energy density decay rate with the frequency of high-frequency tail becomes slightly higher with fetch.

The evolution of wave spectra with wind speed and fetch associated with fetch and duration-limited conditions is shown in Fig. 5. The spectra evolution with wind speed can be seen following the columns of a single row. The spectra evolution with fetch can be observed in the different colors of each panel. The wind speed and fetch evolution are presented for five experiments (rows). The spectra evolution with fetch under constant wind conditions of 6, 9.5, and 13 m s^{-1} was also examined (not shown). The spectral shape evolution with fetch under low acceleration wind conditions of 6, 9.5, and 13 m s^{-1} (experiment 1), are similar to the spectral shape evolution with fetch under the same constant wind speeds; hence they can be used as a reference

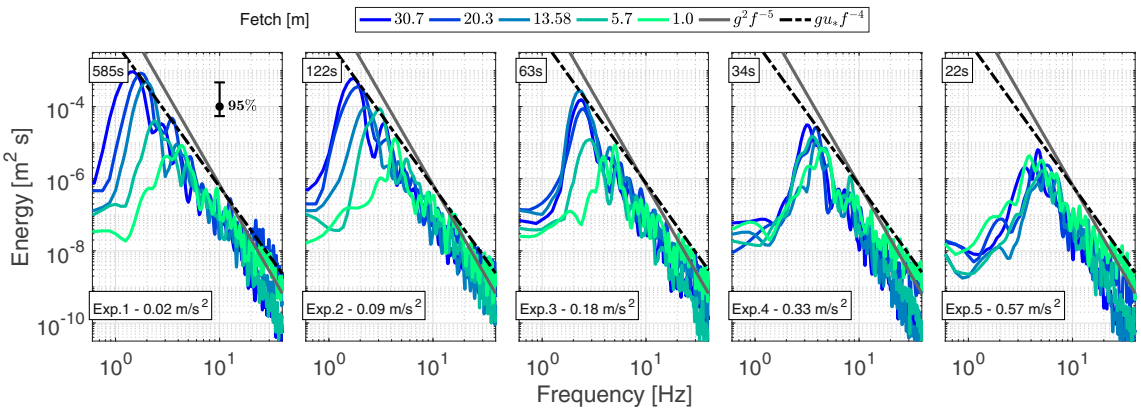

Fig. 4 Wave energy spectrum evolution with fetch for each experiment under 13 m s^{-1} maximum wind speed. The different colors belong to five stations along the wave tank. The solid gray line corresponds to Phillips (1958) formulation, $g^2 f^{-5}$. The dotted black line corresponds to Toba (1973) formulation, $g u_* f^{-4}$. The acceleration associated with each experiment is indicated. The acceleration period duration is also included in each panel

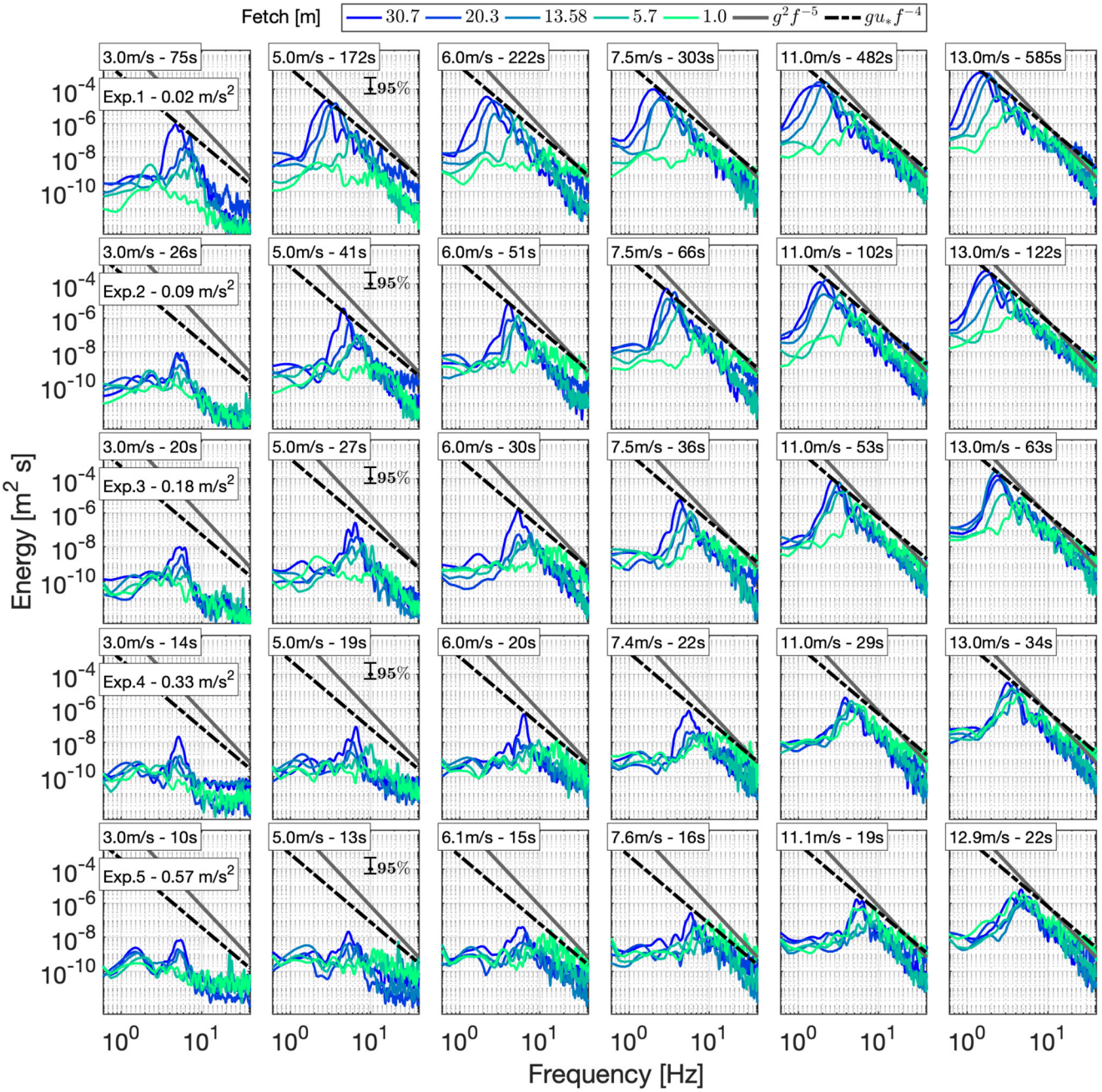

Fig. 5 Wave energy spectrum evolution with wind speed and fetch for each experiment. The different colors belong to five stations along the wave tank. The solid gray line corresponds to Phillips (1958) formulation, $g^2 f^{-5}$. The dotted black line corresponds to Toba (1973) formulation, $gu_* f^{-4}$. The acceleration associated with each experiment is shown. The mean wind speed and time-lapse from the beginning of the acceleration period associated with each panel are included

of constant wind conditions. The wind acceleration effect does not influence the spectral shape evolution with wind speed and fetch under low acceleration wind conditions, but it does under the other accelerated conditions. When the spectral shape associated with constant wind conditions is not reached for a given wind speed under accelerated wind conditions, it could be due to the combined effect of wind acceleration and time as a limiting factor for wave generation. A limitation of the spectral shape evolution with fetch was also observed. The higher the spectral shape evolution limitation with wind speed, the higher the spectral shape evolution limitation with fetch. The limitation with wind speed could be associated with a time limitation, as already mentioned, but the observed limitation

with fetch is independent of time. This last fact proofs that the acceleration magnitude plays a role in limiting wavefield growth under accelerated wind conditions. Wave growth efficiency differences were shown previously in Robles-Diaz et al. (2019), where it was observed that under moderate-low and moderate acceleration wind conditions (experiments 2 and 3), the efficiency of the wavefield capturing the available momentum was the highest.

4 Time series analysis

The time series of significant wave height, H_s, dominant wave steepness, η_x, dominant frequency, f_p, and dominant wavelength, λ_p as observed at three stations (columns) with fetch equal to 2.80, 20.29, and 30.72 m, respectively, during the five experiments (rows) are presented in Fig. 6. The time evolution of 10 m wind speed, U_{10}, as observed at station 7, is also shown, and it is considered constant along

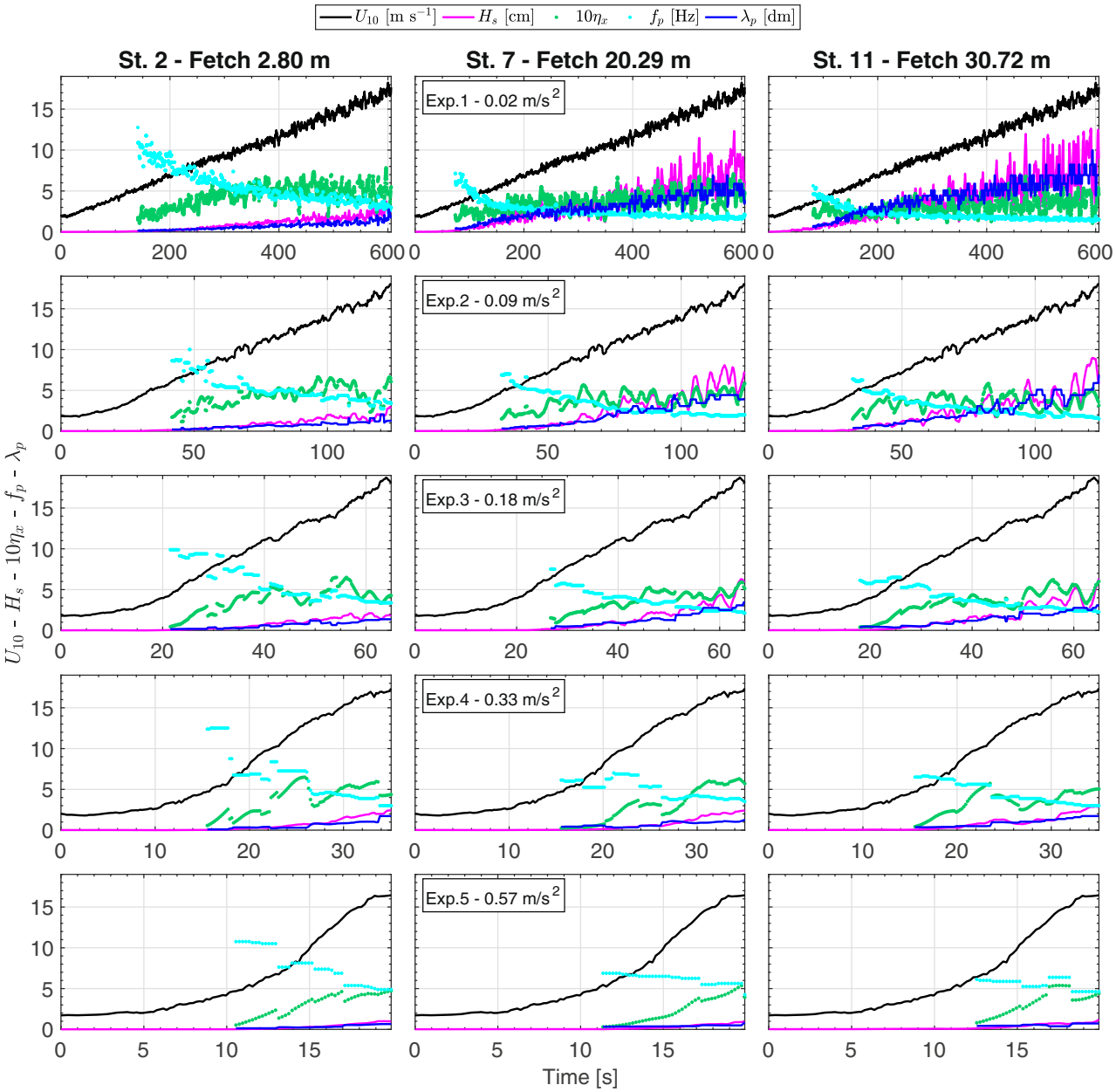

Fig. 6 Time series results for 10 m wind speed, significant wave height, wave steepness, dominant frequency and dominant wavelength from measurement at three stations (2, 7 and 8, with fetch equal to 2.80, 20.29, and 30.72 m respectively), during the five experiments (rows). The acceleration associated with each experiment is indicated

the whole tank. The significant wave height was calculated as four times the standard deviation of surface elevation (Holthuijsen 2007), over a 4 s window. The dominant frequency was computed from the power spectrum (Fig. 5) as the associated with the spectral peak. The dominant wavelength was estimated from the dominant frequency following the linear dispersion relation for gravity-capillary waves. The dominant wave steepness was estimated from the frequency spectrum E_{η_t} of the time derivative of the water surface height signal η_t, as:

$$\eta_x = \frac{2}{c_p}\sqrt{\int E_{\eta_t}(f)df} \tag{1}$$

where the measured dominant phase speed is $c_p = \lambda_p f_p$. The integral is performed over the frequency range $0.5 f_p < f < 1.5 f_p$ (Caulliez et al. 2008).

In Fig. 6, it can be observed that during the experimental runs the characteristics of first detected waves, as well as other wave field variables, not only they do depend on wind speed and fetch, but also on wind acceleration. In general terms significant wave height, peak wavelength and wave steepness tend to increase during the accelerated wind stage of the experiment, while the dominant frequency tends to decrease, regardless of the wind acceleration. Nevertheless, their evolution in time is slightly different depending on the acceleration wind conditions. The main characteristics of the first measurable wave field are similar. However, the first measurable waves are steeper under low and moderate-low acceleration wind conditions (experiments 1 and 2). The wave field main variables are similar under low, moderated-low and moderated acceleration wind conditions (experiments 1, 2, and 3), under the maximum wind speed. For that reason, it could be said that under moderated wind acceleration conditions, experiments 2 and 3, the growth efficiency of the wavefield is higher than low acceleration wind conditions, which takes more time to develop. The growth efficiency is also higher than under moderate-high and high acceleration wind conditions (experiments 4 and 5), where the growth is limited by a combination of time and wind acceleration.

The high variability observed during some variables time series, H_s or λ_p, is probably a response to the high variability that the wind field presents under low and moderate acceleration wind conditions. That also implies more turbulence and more amount of available momentum. In Robles-Diaz et al. (2019) it was shown that once the rough flow conditions are established, the wavefield generated under moderate acceleration wind conditions induces the increase of the available momentum under a certain wind speed.

The wavefield development with fetch is readily apparent during low acceleration wind conditions and short fetches, i.e., the differences between wavefield variables are more significant between stations 2 and 7 (short and moderate fetch, respectively). The effect of fetch is observed to be reduced under high acceleration wind conditions and at stations with long fetches, (a fact that was also identified from the spectral analysis results). These variations related to fetch effect are probably related to the available momentum amount and the wavefield efficiency capturing this momentum under the different acceleration wind conditions.

5 Wave age and drag coefficient

Under accelerated wind conditions, the surface roughness and wave characteristics evolve rapidly with wind speed, and their relation to wind stress is essential to understand the momentum transfer process better (Robles-Diaz et al. 2019). This section shows the relationship between the wind stress in the form of drag coefficient, and the wave phase speed and wave age. The 10 m height drag coefficient, $C_{D_{10}}$, as a function of wind speed is shown in Fig. 7 with the correspondent values of wave celerity, c_p. The same behavior of $C_{D_{10}}$with the correspondent values of wave age is shown in Fig. 8. The X wire probe measurements were used to determine the total wind stress directly, $\tau = \rho u_*^2 = -\rho(\overline{u'w'})$, over the water surface through the eddy-covariance method (Stull 1988) using a 2 s moving window. ρ is the air density, and u' and w' are the horizontal and vertical turbulent components of wind speed, respectively. The drag coefficient is calculated from the estimation of the total wind stress throw the following equation ($|\tau| = \rho C_{D_{10}} U_{10}^2$). The variation $C_{D_{10}}$ of as function of U_{10} is determined as a bin average with a class interval equal to 1 m s^{-1} in the wind speed. The standard deviation of $C_{D_{10}}$ within each class is included together with the estimations.

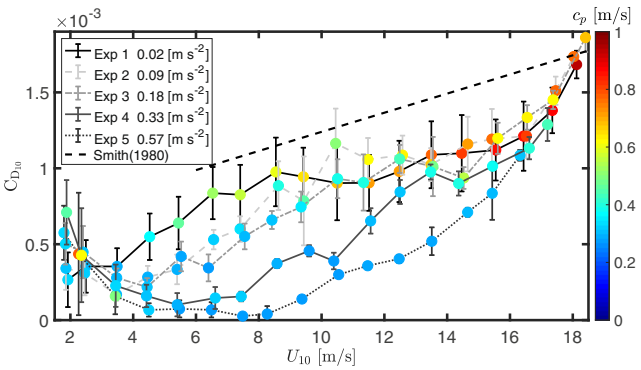

Fig. 7 Behavior of 10 m drag coefficient, $C_{D_{10}}$, as a function of wind speed and with correspondent wave celerity, c_p (color dots). Lines correspond to each experiment with a characteristic wind acceleration value

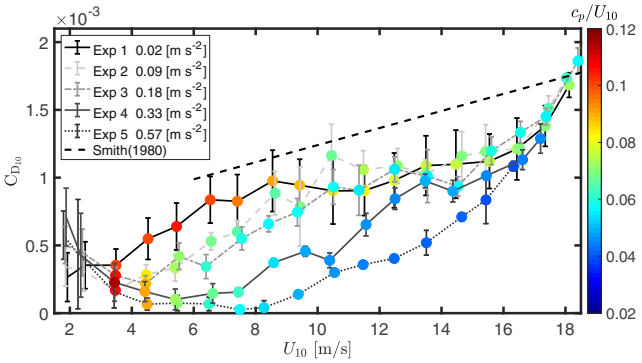

Fig. 8 Behavior of 10 m drag coefficient, $C_{D_{10}}$, as a function of wind speed and with correspondent wave age c_p/U_{10} (color dots). Lines correspond to each experiment with a characteristic wind acceleration value

The wave age is calculated from wave celerity and mean wind speed as c_p/U_{10}.

Wave celerity of the first detected wind waves is around 0.23 m s^{-1} in all experiments. This initial value of phase speed has been observed regardless of wind acceleration. Both phase speed and drag coefficient increase with wind speed. However, this increase is particularly noticeable during low acceleration wind conditions. Then, for certain wind speeds, the wave field under lower acceleration wind conditions shows a higher phase speed, associated with a more developed wave field than under higher acceleration wind conditions (Fig. 7).

It is presumed that the wind acceleration could directly affect the phase speed, i.e., acceleration wind conditions could increase the wave phase speed and the water particle horizontal velocity and promote premature wave breaking. The results of the change in phase speed when wind speed increases from 10 to 17 m s^{-1} are shown in Table 3. This phase speed change is more significant under moderate-low and moderate acceleration wind conditions (experiments 2 and 3) than those with low acceleration wind conditions (experiment 1). Then, under moderate acceleration wind conditions, the waves could prematurely break and generate

Table 3 Results of phase speed of the observed waves at station 7 when wind speed is $U_{10} = 10$ and 17 m s^{-1}, during each of the five experimental runs

Exp.	$C_p(U_{10} = 10$ m s$^{-1})$ [m s^{-1}]	$C_p(U_{10} = 17$ m s$^{-1})$ [m s^{-1}]	$\frac{\Delta C_p}{\Delta U_{10}}$
1	0.592	0.751	0.023
2	0.435	0.725	0.041
3	0.332	0.567	0.034
4	0.277	0.401	0.018
5	0.277	0.317	0.006

Rate of change between phase speed and wind speed is also shown

flow separation in the air boundary layer, increasing wind stress. This process could explain the high values of the drag coefficient associated with the highest wind speeds under moderate-low and moderate acceleration wind conditions (experiments 2 and 3). This drag coefficient increase happens under moderate wind speeds, which generates the maximum value of the drag coefficient associated with the maximum wind speed at the end of the acceleration period.

Wave age values observed in the experiments range from 0.02 to 0.12, corresponding to very young waves ($c_p/U_{10} < 1.2$) since the observed phase speed is much less than the mean wind speed (Fig. 8). Therefore, waves continuously support stress from wind during the whole accelerated wind period. A slight decrease in wave age can be observed under almost every acceleration wind conditions, as both wind speed and drag coefficient increase. This fact indicates that the increase in the mean wind speed is faster than the increase in dominant wave celerity. However, the wave age value is almost constant for wind speeds higher than 6 m s^{-1} under moderate-low and moderate acceleration wind conditions (experiments 2 and 3). That means that the change of wind speed is proportional to the change of wave celerity. This proportionality is maintained under higher wind speeds, which could induce a higher wave efficiency to grow or capture the available momentum.

6 Summary

The generation process of wind waves under accelerated wind conditions was studied from experimental runs carried out in a large wind-wave facility. The laboratory experiments were designed to characterize the wind-wave evolution with wind speed and fetch under different accelerated wind conditions. High-sampling rate devices were installed along the facility to describe the airflow and the water surface vertical displacement. The air-water momentum flux was directly computed using the eddy covariance method with hot-wire anemometry data at the airside. The surface displacement along the wave tank was measured with capacitance and resistance wire probes. The complete set of measurements enables the study of the role of wind acceleration in the momentum transfer between air and water and how the energy is distributed in the wavefield during the early stages of wind-wave development.

These experiments are an initial simplified approximation to study how wind-wave generation could be under accelerated wind conditions in nature. The conditions simulated in the lowest acceleration wind experiment, with a wind acceleration around 0.02 m s^{-2}, could be taking place in the open ocean, such as associated with the entry of a cold front in the Gulf of Mexico. During other wind systems, as *Tehuano* winds at Gulf of Tehuantepec or *Mistral* winds of

Gulf of Lion, a wind speed increase with similar wind acceleration patterns can be observed. The moderate and high acceleration wind conditions could represent accelerations more similar to gusts. More field data research is needed to conclude whether these results can be extrapolated to wider fetches in the ocean. However, it was observed that drag coefficient behavior associated with hurricane wind conditions simulated in laboratory experiments presents a similar behavior in the field (Donelan et al. 2004). It is expected that the wind-waves spectral shape evolution to be similar for fetches similar to those in the laboratory.

The main reason why the acceleration is influencing the evolution of the spectral shape is that it also modifies the amount of momentum available in the air for the wind-wave generation process. Wind speed measurements show that the turbulent fluctuations amplitude increases as the wind acceleration decreases for each experiment. That translates into a high level of turbulence under low, moderate-low and moderate acceleration wind conditions, given a certain wind speed. That effect is indirectly observed in the high variability of wind speed and significant wave and the relatively high drag coefficient values under low, moderate-low, and moderate acceleration wind conditions.

Apart from the differences in the amount of moment induced by the wind acceleration, the waves showed higher efficiency capturing the air momentum under low, moderate-low, and moderate wind acceleration conditions (experiments 1, 2, and 3), associated with the wavefield characteristics (Robles-Diaz et al. 2019). One characteristic that could induce this high efficiency is the higher wave steepness observed under low, moderate-low, and moderate acceleration wind conditions than higher acceleration wind conditions, as reflected in higher high-frequencies energy levels. The high momentum capture efficiency observed in low acceleration wind conditions (experiment 1) is reflected in its spectral energy evolution with wind speed and fetch. The spectral shape shows the same spectral energy distribution obtained under constant wind conditions for a given wind speed and fetch.

Once the rough flow regime is established, the wavefield induces a modification in the increasing tendency of drag coefficient with wind speed (Robles-Diaz et al. 2019). It was observed that under moderate-low and moderate acceleration wind conditions (experiments 2 and 3), the change in phase speed with wind speed is more significant than under the other acceleration wind conditions. That change could induce premature breaking and, therefore, airflow separation and increase wind stress. Furthermore, these experiments show constant wave age values from low wind speeds, i.e., a proportional relationship in the phase speed and wind speed change. This fact could increase the wavefield efficiency of capturing the available air momentum. The combination of both processes could explain that, for maximum wind speed, at the end of the acceleration period, the main wavefield variables present the same magnitude of low acceleration wind conditions and the spectral shape is closer to the one associated with constant wind conditions, i.e., a similar state of wave development is reached in less time.

The spectral shape evolution with fetch also reflects the effect of the wind acceleration magnitude in the amount of available momentum and the wave efficiency to capture this momentum. Under moderate-high and high acceleration wind conditions, these processes are reduced, and the wavefield growth with fetch is not observed.

The turbulent boundary layer evolution under different accelerated wind conditions was characterized in a previous analysis of this data set. The momentum availability was also related to the wave growth process, from a non-dimensional wave growth analysis (Robles-Diaz et al. 2019). In this paper, some wavefield-associated variables, as phase speed and wave age, are related to the drag coefficient evolution with wind speed under accelerated wind conditions. Furthermore, the wavefield evolution is analyzed from a detailed description of the wind-wave spectral shape. The spectral shape evolution is also linked with the amount of momentum and the wave efficiency to capture this momentum.

A more remarkable increase in the saturation level of high frequencies and peak frequency downshifting, as wind speed and fetch increases, was observed under low acceleration wind conditions. Under these acceleration wind conditions, it was also observed a broader spectral peak as wind speed and fetch increases. Wind wave energy spectra showed a broader spectral peak with wind speed and fetch under low acceleration wind conditions. In contrast, under high acceleration wind conditions, the energy saturation level enhancement at relatively high frequencies is less evident. The peak frequency downshift process was not observed as wind speed and fetch increased. Under those high acceleration wind conditions, the wavefield development is somehow inhibited; wind waves do not grow as expected, and their energy level is saturated instead.

Acknowledgements This work represents a contribution of RugDiS-Mar Project (CONACYT 155793), of CONACYT CB-2015-01 255377 Project, and the Gulf of Mexico Research Consortium (CIGoM). Some part of this research work has been carried out within the framework of the Labex MEC. We express our gratitude to L.A. Julieta Castro for her administrative and logistic coordination support. Funding from Excellence Initiative of Aix-Marseille University - A*MIDEX, a French "Investissements d'Avenir" program, and from CONACYT-SENER-Hidrocarburos Project 201441, is greatly acknowledged. LR-D wishes to express her gratitude to CONACYT and the Physical Oceanography Department for the support provided as a Ph.D. scholarship.

References

Caulliez G, Makin V, Kudryavtsev V (2008) Drag of the water surface at very short fetches: Observations and modeling. J Phys Oceanogr 38(9):2038–2055. https://doi.org/10.1175/2008JPO3893.1, https://journals.ametsoc.org/jpo/article-pdf/38/9/2038/4499645/2008jpo3893_1.pdf

Coantic M, Ramamonjiarisoa A, Mestayer P, Resch F, Favre A (1981) Wind-water tunnel simulation of small-scale ocean-atmosphere interactions. J Geophys Res Oceans 86(C7):6607–6626. https://doi.org/10.1029/JC086iC07p06607

Donelan MA, Haus BK, Reul N, Plant WJ, Stiassnie M, Graber HC, Brown OB, Saltzman ES (2004) On the limiting aerodynamic roughness of the ocean in very strong winds. Geophys Res Lett 31(18):1–5. https://doi.org/10.1029/2004GL019460

Fabrikant A (1976) Quasilinear theory of wind wave generation. Izv Akad Nauk Sssr Fiz Atmosfery I Okeana 12(8):858–862

Holthuijsen LH (2007) Waves in oceanic and coastal waters. Cambridge University Press, Cambridge. https://doi.org/10.1017/CBO9780511618536

Janssen PA (1982) Quasilinear approximation for the spectrum of wind-generated water waves. J Fluid Mech 117:493–506

Jeffreys H (1925) On the formation of water waves by wind. Proc R Soc Lond A 107:189–206

Kawai S (1979) Generation of initial wavelets by instability of a coupled shear flow and their evolution to wind waves. J Fluid Mech 93(4):661–703. https://doi.org/10.1017/S002211207900197X

Miles JW (1957) On the generation of surface waves by shear flows. J Fluid Mech 3(02):185–204. https://doi.org/10.1017/S0022112057000567

Mitsuyasu H, Rikiishi K (1978) The growth of duration-limited wind waves. J Fluid Mech 85(04):705–730. https://doi.org/10.1017/S0022112078000889

Phillips OM (1957) On the generation of waves by turbulent wind. J Fluid Mech 2:417–445

Phillips OM (1958) The equilibrium range in the spectrum of wind-generated waves. J Fluid Mech 4:426–434

Robles-Diaz L, Ocampo-Torres FJ, Branger H, Garcia-Nava H, Osuna P, Rascle N (2019) On the early stages of wind-wave generation under accelerated wind conditions. Eur J Mech B/Fluids 78:106–114. https://doi.org/10.1016/j.euromechflu.2019.06.007, http://www.sciencedirect.com/science/article/pii/S0997754618306952

Stull RB (ed) (1988) An introduction to boundary layer meteorology. Springer, Netherlands. https://doi.org/10.1007/978-94-009-3027-8

Toba Y (1973) Local balance in the air-sea boundary processes iii. on the spectrum of wind waves. J Oceanographical Soc Jpn 29(2):209–220. https://doi.org/10.1007/BF02109506

Toba Y, Ebuchi N (1991) Sea-surface roughness length fluctuating in concert with wind and waves. J Oceanographical Soc Jpn 47:63–79

Toba Y, Okada K, Jones ISF (1988) The response of wind-wave spectra to changing winds. part i: Increasing winds. J Phys Oceanogr 18(9):1231–1240. https://doi.org/10.1175/1520-0485(1988)018⟨1231:TROWWS⟩2.0.CO;2

Waseda T, Toba Y, Tulin MP (2001) Adjustment of wind waves to sudden changes of wind speed. J Oceanogr 57:519–533

Zavadsky A, Shemer L (2017) Water waves excited by near-impulsive windÂ forcing. J Fluid Mech 828:459–495. https://doi.org/10.1017/jfm.2017.521